CCS Chemistry

RESEARCH ARTICLE

Received: Oct. 17, 2020 | Accepted: Jan. 29, 2021

Theory-Driven Design of Electrocatalysts for the Two-Electron Oxygen Reduction Reaction Based on Dispersed Metal Phthalocyanines

Yang Wang[1†], Zisheng Zhang[2†], Xiao Zhang[3*], Yubo Yuan[1], Zhan Jiang[1], Hongzhi Zheng[1], Yang-Gang Wang[2], Hua Zhou[4] & Yongye Liang[1,5*]

[1]*Department of Materials Science and Engineering, Southern University of Science and Technology, Shenzhen 518055,* [2]*Department of Chemistry, Guangdong Provincial Key Laboratory of Catalysis, Southern University of Science and Technology, Shenzhen 518055,* [3]*State Key Laboratory of Clean Energy Utilization, Zhejiang University, Hangzhou 310027,* [4]*X-Ray Science Division, Advanced Photon Source, Argonne National Laboratory, Lemont, IL 60439,* [5]*Guangdong-Hong Kong-Macao Joint Laboratory for Photonic-Thermal-Electrical Energy Materials and Devices, Southern University of Science and Technology, Shenzhen 518055*

**Corresponding authors: liangyy@sustech.edu.cn; zhangx_energy@zju.edu.cn;* [†]Y. Wang and Z. Zhang contributed equally to this work.

Cite this: *CCS Chem.* **2021**, *3*, 585–593

The two-electron electrochemical reduction of oxygen is an appealing approach to produce hydrogen peroxide. Metal and heteroatom-doped carbon (M–X/C) materials have recently been recognized as compelling catalysts for this process, but their performance improvement is generally hindered by the ill-defined structures of active sites. Herein, we demonstrate a theory-driven design of catalysts for oxygen reduction reactions based on molecularly dispersed electrocatalysts (MDEs) with metal phthalocyanines on carbon nanotubes. Density functional theory calculations suggest that nickel phthalocyanine (NiPc) favors the formation of *H_2O_2 over *O, thus acting as a selective catalyst for peroxide production. NiPc MDE shows high peroxide yields of ~83%, superior to the aggregated NiPc and pyrolyzed Ni–N/C catalysts. The performance is further enhanced by the introduction of the cyano group (CN). NiPc–CN MDE exhibits ~92% peroxide yields and good stability. Our studies provide a new perspective for the development of heterogeneous electrocatalysts for hydrogen peroxide production from metal macrocyclic complexes.

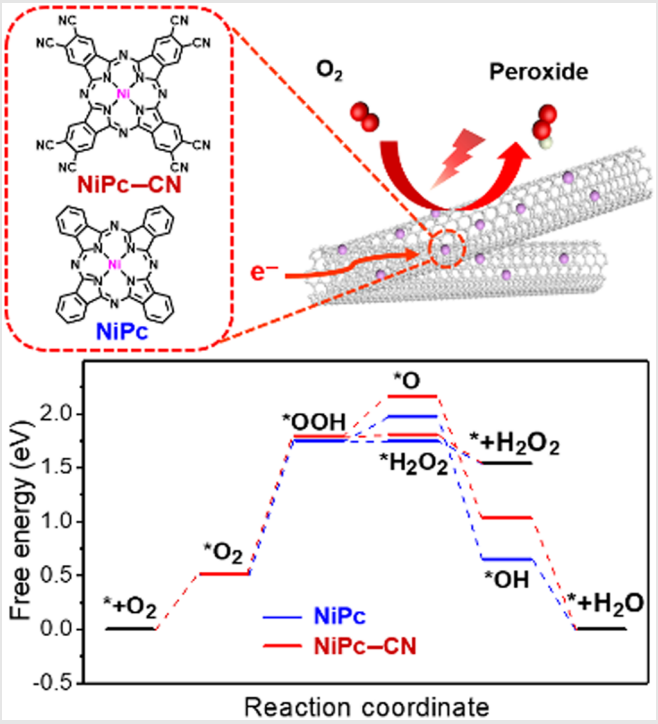

Keywords: metal phthalocyanine, oxygen reduction reaction, peroxide, theory-driven design, molecular engineering

DOI: 10.31635/ccschem.021.202000590
CCS Chem. **2021**, *3*, 585–593

Introduction

Driving economically important chemical reactions with renewable electricity offers an intriguing opportunity to replace current energy-intensive processes.[1-3] For example, the electrochemical oxygen reduction reaction (ORR) through the two-electron ($2e^-$) pathway is considered an environmentally benign alternative to the industrial anthraquinone method to produce hydrogen peroxide (H_2O_2), which is widely used as a green oxidizer in bleaching, waste water treatment, and the chemical industry.[4-6] An ideal electrocatalyst should possess high activity toward the $2e^-$ pathway to the peroxide product and suppress the competing $4e^-$ process to water. Platinum (Pt) or palladium (Pd) alloys with mercury (Hg) have been demonstrated as selective electrocatalysts for the $2e^-$ pathway in ORR.[7,8] However, due to the toxicity of Hg and the limited reserve of noble metals, these elements are not preferred for practical applications.

Carbon-based materials doped with earth-abundant elements, however, are compelling candidates as efficient and affordable electrocatalysts.[9-14] Carbon nanotube (CNT), graphene, and activated carbon with oxygen-containing functional groups were reported to be selective in $2e^-$ ORR.[15-18] Embedding coupled boron–nitrogen (BN) domains into graphitic carbon showed enhanced selectivity and activity for reducing O_2 to HO_2^- compared with the catalysts with individual B or N doping.[19] In addition to metal-free catalysts, metal and heteroatom-doped carbon (M–X/C) catalysts with isolated heteroatom-coordinated metal moieties, one type of single-atom catalysts (SACs), have also been exploited for H_2O_2 production.[20-23] A series of M–N/C (M = Mn, Fe, Co, Ni, and Cu) catalysts with proposed M–N_4 active sites were synthesized to investigate their performance in ORR. The Co–N/C catalyst showed preference for the $2e^-$ pathway in acidic condition.[24] Moreover, SACs with transition-metal centers coordinated by different heteroatoms, such as O and S, were also reported to show high selectivities for the $2e^-$ reduction pathway in ORR.[25-28] However, the lack of well-defined structures and the copresence of various types of active sites prevent understanding the structure–performance relationships and catalyst design principles in these SAC catalysts.

Metal macrocyclic complexes, such as metal phthalocyanines (MPcs) and porphyrins with well-defined M–N_4 moieties, have been attractive electrocatalysts since the report of cobalt phthalocyanine as an active ORR catalyst.[29-31] For instance, iron phthalocyanine (FePc) has been reported to be efficient in catalyzing ORR through the $4e^-$ pathway to water.[32,33] However, the performances of metal complexes in heterogeneous form are often limited by their low electric conductivity.[34-36] Hybridizing metal macrocyclic complexes with nanocarbon materials were found to promote their catalytic performances.[35,37,38] In the carbon dioxide reduction reaction, achieving molecular dispersion on conducting supports is beneficial to reveal the intrinsic performance of molecular catalysts and establish catalyst design principles.[39,40] In addition, previous reports of heterogeneous molecular ORR catalysts mainly focused on optimizing the performance toward the $4e^-$ pathway with little exploration of the $2e^-$ pathway to peroxide production.[30,41]

In this work, we present a theory-driven design of electrocatalysts based on an molecularly dispersed electrocatalyst (MDE) consisting of dispersed MPcs on CNTs for electrochemical production of peroxide. From density functional theory (DFT) calculations, we identify nickel phthalocyanine (NiPc) as a selective catalyst for $2e^-$ ORR with experimental peroxide yields of ~83% in the form of MDE, in contrast to FePc MDE that is selective for $4e^-$ ORR. Achieving molecular dispersion of NiPc with well-defined Ni–N_4 sites is important to the high peroxide selectivity as proven by the lower peroxide yields of the physically mixed NiPc and CNT (containing aggregated NiPc) and a pyrolyzed Ni–N/C SAC. Moreover, molecular engineering of NiPc MDE with the introduction of cyano groups (CNs) to the Pc ligand (NiPc–CN MDE) further enlarges the free-energy preference to the $2e^-$ pathway and enhances the selectivity for the electrochemical production of peroxide. NiPc–CN MDE exhibits a high peroxide yield of ~92% in the potential range of 0.70–0.20 V versus a reversible hydrogen electrode (RHE).

Experimental Methods

Preparation of MPc MDEs

The preparation of MPc MDEs was based on a reported procedure with the control of the ratio between MPcs and CNTs.[40] NiPc and FePc were obtained from commercial sources, and NiPc–CN was synthesized according to a reported method.[40] Briefly, 30 mg purified CNTs were dispersed in 25 mL of *N*,*N*-dimethylformamide (DMF) with the assistance of sonication, in which a calculated amount of MPcs in 5 mL of DMF was added to obtain a well-mixed suspension. The mixture was further sonicated for 30 min and then stirred at room temperature for 20 h. Subsequently, the precipitate was collected by centrifuge and washed with DMF (three times) and ethanol (twice). Finally, the collected precipitate was lyophilized to yield the final product.

Electrochemical measurements

About 4 mg of MPc MDEs and 10 μL of 5 wt % Nafion solution were dispersed in 990 μL ethanol under ultrasonication to form a homogeneous ink. About 13 μL catalyst ink was loaded onto the glassy carbon (GC) disk electrode (5.5 mm in diameter) of a rotating ring-disk electrode (RRDE) to achieve a catalyst loading of ~0.2 mg cm^{-2}. The ink of NiPc + CNT was prepared by

DOI: 10.31635/ccschem.021.202000590
CCS Chem. **2021**, *3*, 585–593

dispersing 2.8 mg of NiPc, 1.2 mg of CNT, and 10 μL of 5 wt % Nafion solution in 990 μL ethanol under ultrasonication, then loaded onto the GC electrode. The RRDE experiments were conducted with a four-electrode system using a saturated calomel electrode (SCE) as the reference electrode (calibrated with a homemade RHE), a graphite rod as the counter electrode, and the catalyst-modified GC disk electrode as the working electrode. Meanwhile, the Pt ring electrode was kept at 1.5 V (vs RHE, the same for following potentials unless otherwise stated) for all experiments. The disk and ring electrodes were rotated at a speed of 1600 rpm (Pine research). Electrolytes (0.1 M KOH) were saturated with O_2 by bubbling for 30 min prior to each experiment, and a flow of O_2 was maintained over the electrolyte during the reaction. Linear sweep voltammetry (LSV) was conducted by scanning the disk electrode potential with a scan rate of 5 mV/s. For the stability test, the disk electrode potential was kept at 0.5 V. Experiments were also performed under an argon environment to record the background currents of the disk and ring electrodes, which were subtracted from the currents under O_2. The peroxide yield and electron transfer number (n) were determined by the following equations:

$$\text{Peroxide yield } (HO_2^-) = 200\times\frac{(I_r/N)}{I_d+(I_r/N)}\%$$

$$n = 4\times\frac{I_d}{I_d+(I_r/N)}$$

where I_r is ring current, I_d is disk current, and N is current collection efficiency of the Pt ring electrode (0.28, calibrated with $K_3[Fe(CN)_6]$).

Computational Methods

DFT calculations of gas-phase MPc molecules catalyzing ORR were conducted using the Gaussian 09 program.[42] B3LYP functional[43] with D3 correction (Becke–Johnson damping)[44] was adopted for calculation.[45] The all-electron 6-31G* basis set (for H, C, N, and O)[46-48] and the Stuttgart–Dresden (SDD) basis set containing all double-ξ valence with effective core potentials (ECPs)[49] (for Ni and Fe) were used. The geometric structures were all optimized at 298.15 K and under 1 atm. The harmonic vibrational frequencies were computed with no imaginary frequency found for all reaction intermediates. The Gibbs free energies of high- and low-spin forms of all intermediates were calculated with the harmonic potential approximation to determine the ground states. The electrocatalytic mechanisms were investigated with the computational hydrogen electrode (CHE) model.[50] Additional details of computational methods are available in the Supporting Information.

Results and Discussion

Theoretical calculations of MPcs catalyzing ORR

To understand how the central metals in MPc molecules affect the product selectivity in ORR, DFT calculations of the free-energy changes of ORR through the $2e^-$ and $4e^-$ pathways were conducted on FePc and NiPc at 1.23 V versus RHE. The calculated free-energy diagrams suggest distinctly different ORR behaviors of FePc and NiPc (Figure 1a). On FePc, O_2 is first adsorbed on the Fe center, followed by a proton-coupled electron transfer (PCET) process to form *OOH with an uphill free-energy change. The divergence of the $2e^-$ and $4e^-$ pathways came from the preference of *OOH reduction with a protonation mechanism to $*H_2O_2$ or an O–O cleavage to *O. The downhill free-energy change to form *O and the large free-energy increase required for the generation of $*H_2O_2$ indicate a high preference for the $4e^-$ reduction pathway on FePc, consistent with high selectivities of O_2 reduction

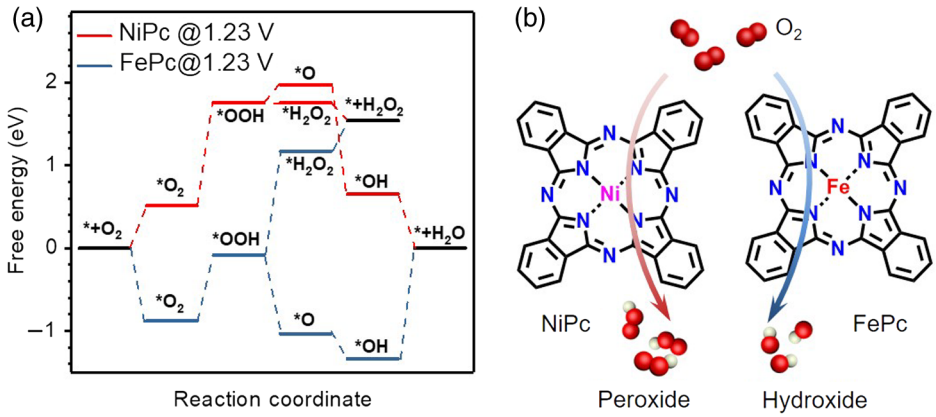

Figure 1 | *Theoretical calculations of ORR catalyzed by MPcs. (a) Calculated free-energy diagrams of ORR through the $2e^-$ and $4e^-$ reduction pathways on NiPc and FePc at 1.23 V. (b) Schematic presentation of ORR selectivity on NiPc and FePc based on DFT calculations.*

DOI: 10.31635/ccschem.021.202000590
CCS Chem. **2021**, *3*, 585–593

to water/hydroxide of Fe macrocyclic complexes and Fe-based SACs in previous reports.[34,51] By contrast, the *OOH intermediate (generated from O_2 through an $*O_2$ intermediate with two uphill free-energy changes) on NiPc shows a slight downhill free-energy change to generate $*H_2O_2$, while the formation of *O in the 4e⁻ reduction pathway is energetically uphill (Figure 1a). In contrast to FePc, the reversed trend in free-energy changes to form $*H_2O_2$ and *O on NiPc suggests the preference for the 2e⁻ reduction pathway. Therefore, NiPc molecules are predicted to be selective electrocatalysts for 2e⁻ ORR to peroxide product (Figure 1b).

ORR performance of MPc MDEs and aggregated MPcs

Dispersed NiPc and FePc molecules were supported on the CNTs via π–π interactions to fabricate MPc MDEs according to our previous method[40] to examine the calculated trends in ORR. The metal contents in MDEs were controlled to be ~0.7 wt % (Supporting Information Table S1), which were measured by inductively coupled plasma mass spectrometry (ICP-MS). The electrochemical behaviors of NiPc MDE and FePc MDE were first investigated in O_2-saturated 0.1 M KOH electrolytes with the RRDE setup (0.2 mg cm^{-2} catalyst loading). The MDEs were drop-coated on the disk electrode as the working electrode to reduce O_2, while the ring electrode (Pt) was maintained at 1.5 V to detect the produced peroxide. FePc MDE shows more positive onset potential (0.94 V at –0.025 mA, corresponding to a current density of ~–0.1 mA cm^{-2}) than that of NiPc MDE (0.79 V) (Figure 2a). The current of FePc MDE is saturated to –1.41 mA at ~0.58 V. The saturation current for NiPc MDE is about –0.63 mA at the same potential. The peroxide yield and *n* of MPc MDEs calculated from the disk and ring currents are depicted in Figure 2b and Supporting Information Figure S1, respectively. NiPc MDE shows good peroxide yields of ~83% in the potential range of 0.70–0.53 V, which decline at more negative potentials. Correspondingly, *n* of NiPc MDE is below 2.34 in the potential range of 0.70–0.53 V, which gradually increases to 2.83 from 0.53 to 0.20 V (Supporting Information Figure S1). In contrast, low peroxide yields of ~1% together with *n* above 3.97 in the potential range of 0.70–0.20 V are observed with FePc MDE (Figure 2b and Supporting Information Figure S1), confirming its strong preference toward the 4e⁻ reduction pathway. These results indicate that the preferred ORR pathways of NiPc MDE and FePc MDE are the 2e⁻ and 4e⁻ reduction pathways, respectively, which are consistent with the DFT calculations (Figure 1a).

The effects of aggregation state of NiPc were further investigated. The NiPc molecules directly deposited on substrates easily formed aggregates due to their strong intermolecular interactions (Supporting Information Figure S2). Due to the poor electric conductivity and limited exposure of active sites of aggregated NiPc, the neat NiPc electrode shows minimal activity in ORR (Figure 2a). Therefore, we physically mixed NiPc with CNTs (denoted as NiPc + CNT) to enhance the conductivity. LSV shows that the physically mixed NiPc + CNT possesses higher activity than that of neat NiPc (Figure 2a). Although NiPc + CNT exhibits even more positive onset potential than NiPc MDE, the low peroxide yields of NiPc + CNT (under 60% in the potential range of 0.70–0.20 V) suggests much less preference toward the 2e⁻ pathway compared with NiPc MDE (Figure 2b). Topological defects and N-dopants have been considered as active sites for ORR.[11] However, Pc MDE (prepared by anchoring Pc molecules on CNTs) without metal centers shows inferior ORR activity and selectivity for the 2e⁻ pathway compared with NiPc MDE (Supporting Information Figure S3). These results suggest the critical

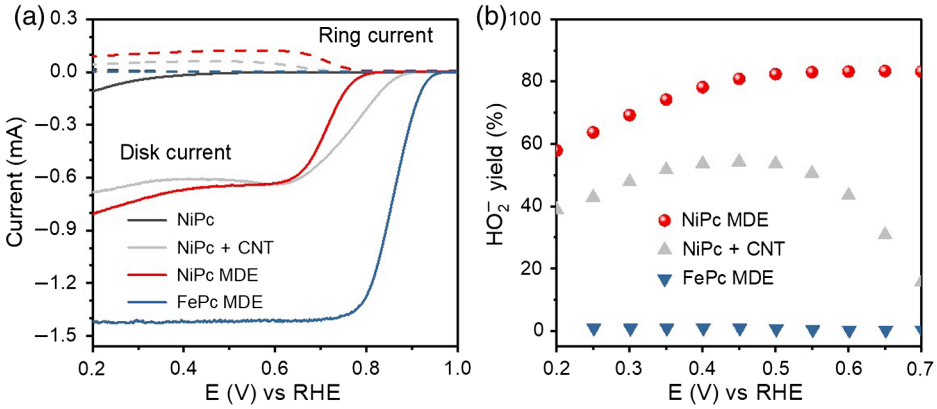

Figure 2 | *ORR performance of MPc-based electrocatalysts on RRDE. (a) Disk and ring currents of NiPc, NiPc + CNT, NiPc MDE, and FePc MDE in O_2-saturated 0.1 M KOH electrolytes on RRDE test rotating at 1600 rpm. (b) Calculated peroxide yields of NiPc MDE, NiPc + CNT, and FePc MDE.*

DOI: 10.31635/ccschem.021.202000590
CCS Chem. **2021**, *3*, 585–593

role of dispersed Ni centers rather than the N-dopants or topological defects in the selective electrocatalysis of 2e⁻ ORR.

To investigate the origin of the different ORR behaviors of neat NiPc, NiPc + CNT, and NiPc MDE, their structures were characterized by scanning electron microscopy (SEM) and transmission electron microscopy (TEM). The TEM (Supporting Information Figure S4a) and SEM (Supporting Information Figure S4b) images of NiPc MDE show the bundles of multiwalled CNTs and excluded the formation of nano- or microsized NiPc aggregates. The isolated bright spots in the high-angle annular dark-field (HAADF) image of NiPc MDE obtained with a Cs-corrected scanning TEM (STEM) indicate the existence of single-Ni sites, suggesting the molecular dispersion of NiPc on CNTs (Supporting Information Figure S5). No appreciable signature peaks of NiPc molecules are observed in the Raman spectrum of NiPc MDE (Supporting Information Figure S6), which could be due to the low content of NiPc in NiPc MDE. On the contrary, physically mixed NiPc + CNT contains microsized NiPc aggregates, as revealed by SEM and confirmed by energy-dispersive spectrometry (EDS) mapping of the Ni signals (Supporting Information Figures S4c and S7).

Electrochemical impedance spectroscopy (EIS) was further conducted to gain insights into the ORR kinetics of the NiPc catalysts in aggregated and dispersed states. The Nyquist plots in Supporting Information Figure S4d show that the charge transfer of NiPc MDE for ORR is more favorable than that of NiPc and NiPc + CNT. The neat NiPc exhibited the largest charge-transfer resistance, in agreement with its low activity from LSV (Figure 2a). It should be noted that DFT calculations with individual NiPc molecule-catalyzing ORR suggest high selectivity toward the 2e⁻ transfer pathway, which is only observed in dispersed NiPc as in NiPc MDE but not in aggregated NiPc as in NiPc + CNT. These results emphasize the importance of correlating free-energy diagrams calculated with individual catalyst molecule with the electrocatalytic performance of dispersed molecular catalysts as opposed to aggregated molecules.

Comparison with the pyrolyzed Ni–N/C SAC

SACs have gained extensive attention recently due to their superior electrocatalytic properties. In electrocatalytic applications, SACs are generally fabricated by pyrolyzing metal salts and N-containing organic precursors at

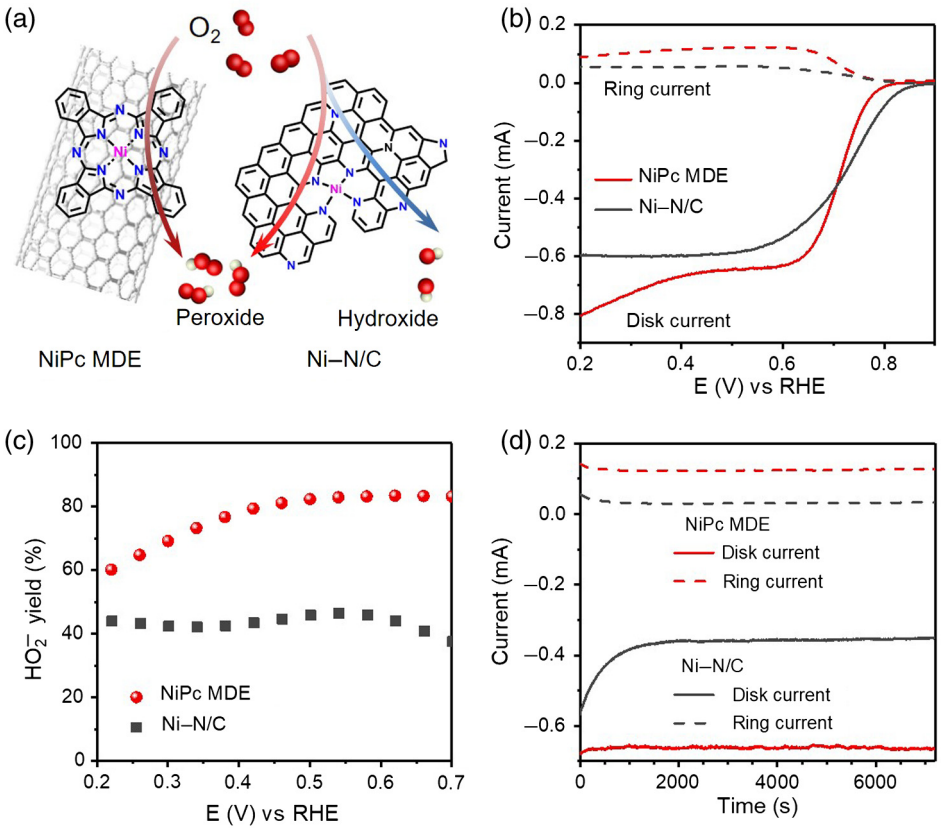

Figure 3 | *Comparison of electrocatalytic ORR performance between NiPc MDE and Ni–N/C. (a) Schematic presentation of ORR with NiPc MDE and Ni–N/C. (b) Disk and ring currents of NiPc MDE and Ni–N/C in O_2-saturated 0.1 M KOH electrolytes. (c) Calculated peroxide yields of NiPc MDE and Ni–N/C. (d) Stability tests of NiPc MDE and Ni–N/C under the constant potentials of 0.50 V for the disk electrode and 1.50 V for the ring electrode.*

DOI: 10.31635/ccschem.021.202000590
CCS Chem. **2021**, *3*, 585–593

high temperatures. However, these pyrolyzed SACs often contain parasitic active sites due to the insufficient structural control during the high-temperature synthesis.[52] For comparison, a nickel SAC with Ni–N_x structures (denoted as Ni–N/C) was synthesized by pyrolyzing a Ni-containing zeolitic imidazolate framework (ZIF) precursor according to the reported method with minor modifications.[53] The Ni content of the Ni–N/C catalyst was also controlled to be ~0.7 wt % (measured by ICP-MS) to compare with NiPc MDE. TEM images of Ni–N/C suggest the absence of metallic Ni particles in the catalyst (Supporting Information Figure S8). The X-ray diffraction (XRD) pattern of Ni–N/C only shows broad features attributable to graphitic carbon (Supporting Information Figure S9),[53] further indicating the absence of metallic Ni or crystalline Ni-containing compounds. The Fourier-transformed extended X-ray adsorption fine structure (FT-EXAFS) curve of Ni–N/C exhibits a peak at ~1.4 Å (without phase correction) corresponding to Ni–N coordination, but little signal at ~2.1 Å corresponding to Ni–Ni coordination (Supporting Information Figure S10), confirming the presence of single Ni sites in Ni–N/C.

Although no Ni particles are observed, parasitic active sites such as N-doped carbon sites could still be present in the Ni–N/C catalyst,[54,55] which are known to be active for 4e⁻ ORR (Figure 3a). The ORR performance of the Ni–N/C catalyst was further characterized in the RRDE setup with identical conditions as NiPc MDE. Given the LSV curves (Figure 3b), Ni–N/C possesses more positive onset potential (0.83 V) than that of NiPc MDE (0.79 V). The peroxide yields of Ni–N/C are under 43% with *n* larger than 3.1 in the potential range of 0.70–0.20 V (Figure 3c and Supporting Information Figure S11). The much worse selectivity of the Ni–N/C catalyst toward the 2e⁻ reduction pathway than that of NiPc MDE is attributed to the structural heterogeneity in the pyrolyzed Ni–N/C catalyst. Additionally, the stability tests were carried out at the constant potentials of 0.50 V for the disk electrode to conduct ORR and at 1.50 V for the ring electrode to detect generated peroxide. As shown in Figure 3d, Ni–N/C shows obvious decay of both the disk and ring currents in the first half hour, suggesting the instability of the pyrolyzed structure. By contrast, NiPc MDE exhibits much better stability without appreciable decay of the disk and ring currents during the measurement. Therefore, the molecularly dispersed and well-defined Ni–N_4 sites in NiPc MDE render it a better ORR catalyst for the 2e⁻ reduction pathway than the pyrolyzed Ni–N/C. NiPc MDE can be a model catalyst

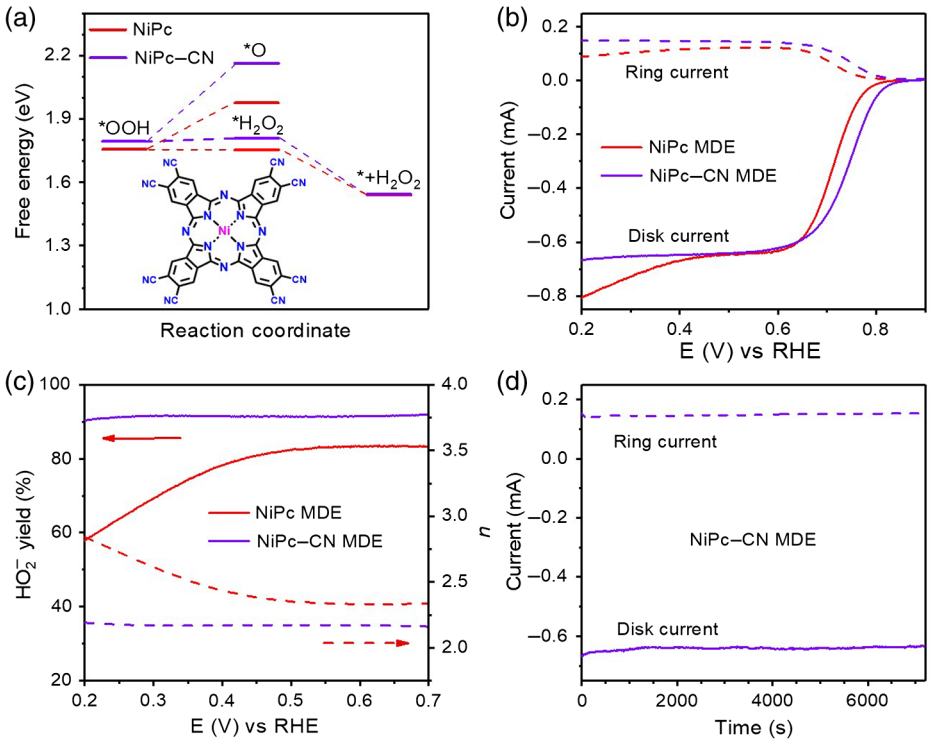

Figure 4 | *Enhanced ORR electrocatalysis with NiPc–CN MDE. (a) Calculated free-energy diagrams of ORR through the 2e⁻ and 4e⁻ reduction pathways on NiPc and NiPc–CN at 1.23 V. Inset shows the molecular structure of NiPc–CN. (b) Disk and ring currents of NiPc and NiPc–CN MDEs in O_2-saturated 0.1 M KOH electrolytes. (c) Calculated peroxide yields and* n *of NiPc and NiPc–CN MDEs. (d) Stability test of NiPc–CN MDE under the constant potentials of 0.50 V for the disk electrode and 1.50 V for the ring electrode.*

DOI: 10.31635/ccschem.021.202000590
CCS Chem. **2021**, *3*, 585–593

system to establish the relationship between the active site structure and electrocatalytic performance.

Molecular engineering of NiPc MDEs for ORR

A unique advantage of the MDE system is the capability of manipulating the properties of the active sites and the associated electrocatalytic performance through molecular engineering. Hence, we seek to further improve the performance of NiPc MDE for $2e^-$ ORR for peroxide production with the introduction of pedant groups to the Pc ligand. We examined NiPc-substituted with electron-withdrawing CNs (NiPc–CN, nickel(II) 2,3,9,10, 16,17,23,24-octacyano-phthalocyanine, see Figure 4a inset for molecular structure) as an ORR catalyst by DFT calculations. The free-energy diagrams suggest that, similar to NiPc, NiPc–CN shows strong preference toward the $2e^-$ reduction pathway, and the energy difference of generating $*H_2O_2$ over *O is enlarged from 0.22 eV with NiPc to 0.37 eV with NiPc–CN (Figure 4a), indicating that NiPc–CN can be a more selective catalyst for $2e^-$ ORR.

NiPc–CN MDE was synthesized (Supporting Information Figure S12) and characterized with the RRDE setup. The LSV curve shows more positive onset potential of NiPc–CN MDE (0.82 V) than that of NiPc MDE (0.79 V) (Figure 4b). Moreover, the saturation current for NiPc–CN MDE remains similar in the potential range of 0.60–0.20 V together with constant ring currents. The peroxide yields of NiPc–CN MDE were calculated to be ~92% from 0.70 to 0.20 V, superior to NiPc MDE with decreased peroxide yields below 0.45 V (Figure 4c). The enhanced peroxide yields of NiPc–CN MDE are consistent with the improved preference toward the $2e^-$ reduction pathway from DFT calculations with the introduction of CNs (Figure 4a). NiPc–CN MDE also shows good stability in ORR with little decay in the disk and ring currents and the peroxide yields during the operation (Figure 4d). The performance of NiPc–CN MDE for oxygen reduction to peroxide is among the best for the reported single-metal and nonprecious metal catalysts, demonstrating high peroxide selectivity of ~92% at a wide potential window in alkaline conditions (Supporting Information Table S2).

Conclusions

Driven by rational catalyst design with DFT calculations, we identify NiPc MDE as a good ORR catalyst for the $2e^-$ reduction pathway and further enhance its performance through molecular engineering. The enhanced NiPc–CN MDE with CN substitution shows superior selectivity with peroxide yield of ~92% in the potential range of 0.70–0.20 V. The molecularly dispersed and well-defined $Ni–N_4$ sites on CNTs endow NiPc MDEs with higher $2e^-$ selectivities than the aggregated NiPc and pyrolyzed Ni–N/C catalysts. These results also imply that the MPc MDE system can act as excellent model electrocatalysts for the establishment of the relationship between active site structures and electrocatalytic performances of molecular catalysts and SACs.

Supporting Information

Supporting Information is available and includes methods, Figures S1–S12, Tables S1 and S2, and References 1–12.

Conflict of Interest

There is no conflict of interest to report.

Funding Information

This work was supported by Guangdong-Hong Kong-Macao Joint Laboratory for Photonic-Thermal-Electrical Energy Materials and Devices (no. 2019B121205001), the startup support from Zhejiang University, and Guangdong Provincial Key Laboratory of Catalysis (no. 2020B121201002).

Acknowledgments

TEM and ICP data were measured with instruments maintained by SUSTech Core Research Facilities. The XAS data were obtained with the resources of the Advanced Photon Source (12-BM), a U.S. Department of Energy (DOE) Office of Science User Facility operated for the DOE Office of Science by Argonne National Laboratory under Contract no. DE-AC02-06CH11357. The computational resource is supported from the Center for Computational Science and Engineering (SUSTech).

References

1. Lewis, N. S.; Nocera, D. G. Powering the Planet: Chemical Challenges in Solar Energy Utilization. *Proc. Natl. Acad. Sci. U. S. A.* **2006**, *103*, 15729–15735.
2. Artero, V. Bioinspired Catalytic Materials for Energy-Relevant Conversions. *Nat. Energy* **2017**, *2*, 17131.
3. De Luna, P.; Hahn, C.; Higgins, D.; Jaffer, S. A.; Jaramillo, T. F.; Sargent, E. H. What Would It Take for Renewably Powered Electrosynthesis to Displace Petrochemical Processes? *Science* **2019**, *364*, eaav3506.
4. Shen, R.; Chen, W.; Peng, Q.; Lu, S.; Zheng, L.; Cao, X.; Wang, Y.; Zhu, W.; Zhang, J.; Zhuang, Z.; Chen, C.; Wang, D.; Li, Y. High-Concentration Single Atomic Pt Sites on Hollow CuS_x for Selective O_2 Reduction to H_2O_2 in Acid Solution. *Chem* **2019**, *5*, 2099–2110.
5. Perry, S. C.; Pangotra, D.; Vieira, L.; Csepei, L.-I.; Sieber, V.; Wang, L.; Ponce de León, C.; Walsh, F. C. Electrochemical Synthesis of Hydrogen Peroxide from Water and Oxygen. *Nat. Rev. Chem.* **2019**, *3*, 442–458.

6. Jiang, K.; Zhao, J.; Wang, H. Catalyst Design for Electrochemical Oxygen Reduction toward Hydrogen Peroxide. *Adv. Funct. Mater.* **2020**, *30*, 2003321.
7. Siahrostami, S.; Verdaguer-Casadevall, A.; Karamad, M.; Deiana, D.; Malacrida, P.; Wickman, B.; Escudero-Escribano, M.; Paoli, E. A.; Frydendal, R.; Hansen, T. W.; Chorkendorff, I.; Stephens, I. E. L.; Rossmeisl, J. Enabling Direct H_2O_2 Production through Rational Electrocatalyst Design. *Nat. Mater.* **2013**, *12*, 1137–1143.
8. Verdaguer-Casadevall, A.; Deiana, D.; Karamad, M.; Siahrostami, S.; Malacrida, P.; Hansen, T. W.; Rossmeisl, J.; Chorkendorff, I.; Stephens, I. E. L. Trends in the Electrochemical Synthesis of H_2O_2: Enhancing Activity and Selectivity by Electrocatalytic Site Engineering. *Nano Lett.* **2014**, *14*, 1603–1608.
9. Yin, P.; Yao, T.; Wu, Y.; Zheng, L.; Lin, Y.; Liu, W.; Ju, H.; Zhu, J.; Hong, X.; Deng, Z.; Zhou, G.; Wei, S.; Li, Y. Single Cobalt Atoms with Precise N-Coordination as Superior Oxygen Reduction Reaction Catalysts. *Angew. Chem. Int. Ed.* **2016**, *55*, 10800–10805.
10. Chen, Y.; Ji, S.; Chen, C.; Peng, Q.; Wang, D.; Li, Y. Single-Atom Catalysts: Synthetic Strategies and Electrochemical Applications. *Joule* **2018**, *2*, 1242–1264.
11. Iglesias, D.; Giuliani, A.; Melchionna, M.; Marchesan, S.; Criado, A.; Nasi, L.; Bevilacqua, M.; Tavagnacco, C.; Vizza, F.; Prato, M.; Fornasiero, P. N-Doped Graphitized Carbon Nanohorns as a Forefront Electrocatalyst in Highly Selective O_2 Reduction to H_2O_2. *Chem* **2018**, *4*, 106–123.
12. Han, L.; Sun, Y.; Li, S.; Cheng, C.; Halbig, C. E.; Feicht, P.; Hübner, J. L.; Strasser, P.; Eigler, S. In-Plane Carbon Lattice-Defect Regulating Electrochemical Oxygen Reduction to Hydrogen Peroxide Production over Nitrogen-Doped Graphene. *ACS Catal.* **2019**, *9*, 1283–1288.
13. Fei, H.; Dong, J.; Chen, D.; Hu, T.; Duan, X.; Shakir, I.; Huang, Y.; Duan, X. Single Atom Electrocatalysts Supported on Graphene or Graphene-Like Carbons. *Chem. Soc. Rev.* **2019**, *48*, 5207–5241.
14. Li, L.; Tang, C.; Zheng, Y.; Xia, B.; Zhou, X.; Xu, H.; Qiao, S.-Z. Tailoring Selectivity of Electrochemical Hydrogen Peroxide Generation by Tunable Pyrrolic-Nitrogen-Carbon. *Adv. Energy Mater.* **2020**, *10*, 2000789.
15. Lu, Z.; Chen, G.; Siahrostami, S.; Chen, Z.; Liu, K.; Xie, J.; Liao, L.; Wu, T.; Lin, D.; Liu, Y.; Jaramillo, T. F.; Nørskov, J. K.; Cui, Y. High-Efficiency Oxygen Reduction to Hydrogen Peroxide Catalysed by Oxidized Carbon Materials. *Nat. Catal.* **2018**, *1*, 156–162.
16. Kim, H. W.; Ross, M. B.; Kornienko, N.; Zhang, L.; Guo, J.; Yang, P.; McCloskey, B. D. Efficient Hydrogen Peroxide Generation Using Reduced Graphene Oxide-Based Oxygen Reduction Electrocatalysts. *Nat. Catal.* **2018**, *1*, 282–290.
17. Sa, Y. J.; Kim, J. H.; Joo, S. H. Active Edge-Site-Rich Carbon Nanocatalysts with Enhanced Electron Transfer for Efficient Electrochemical Hydrogen Peroxide Production. *Angew. Chem. Int. Ed.* **2019**, *58*, 1100–1105.
18. Xia, C.; Xia, Y.; Zhu, P.; Fan, L.; Wang, H. Direct Eelectrosynthesis of Pure Aqueous H_2O_2 Solutions up to 20% by Weight Using a Solid Electrolyte. *Science* **2019**, *366*, 226–231.
19. Chen, S.; Chen, Z.; Siahrostami, S.; Higgins, D.; Nordlund, D.; Sokaras, D.; Kim, T. R.; Liu, Y.; Yan, X.; Nilsson, E.; Sinclair, R.; Norskov, J. K.; Jaramillo, T. F.; Bao, Z. Designing Boron Nitride Islands in Carbon Materials for Efficient Electrochemical Synthesis of Hydrogen Peroxide. *J. Am. Chem. Soc.* **2018**, *140*, 7851–7859.
20. Li, B. Q.; Zhao, C. X.; Liu, J. N.; Zhang, Q. Electrosynthesis of Hydrogen Peroxide Synergistically Catalyzed by Atomic Co-N_x-C Sites and Oxygen Functional Groups in Noble-Metal-Free Electrocatalysts. *Adv. Mater.* **2019**, *31*, 1808173.
21. Choi, C. H.; Kim, M.; Kwon, H. C.; Cho, S. J.; Yun, S.; Kim, H.-T.; Mayrhofer, K. J. J.; Kim, H.; Choi, M. Tuning Selectivity of Electrochemical Reactions by Atomically Dispersed Platinum Catalyst. *Nat. Commun.* **2016**, *7*, 10922.
22. Jia, Y.; Yao, X, Atom-Coordinated Structure Triggers Selective H_2O_2 Production. *Chem* **2020**, *6*, 548–550.
23. Gao, J.; Yang, H. b.; Huang, X.; Hung, S.-F.; Cai, W.; Jia, C.; Miao, S.; Chen, H. M.; Yang, X.; Huang, Y.; Zhang, T.; Liu, B. Enabling Direct H_2O_2 Production in Acidic Media through Rational Design of Transition Metal Single Atom Catalyst. *Chem* **2020**, *6*, 658–674.
24. Sun, Y.; Silvioli, L.; Sahraie, N. R.; Ju, W.; Li, J.; Zitolo, A.; Li, S.; Bagger, A.; Arnarson, L.; Wang, X.; Moeller, T.; Bernsmeier, D.; Rossmeisl, J.; Jaouen, F.; Strasser, P. Activity-Selectivity Trends in the Electrochemical Production of Hydrogen Peroxide over Single-Site Metal-Nitrogen-Carbon Catalysts. *J. Am. Chem. Soc.* **2019**, *141*, 12372–12381.
25. Jiang, K.; Back, S.; Akey, A. J.; Xia, C.; Hu, Y.; Liang, W.; Schaak, D.; Stavitski, E.; Norskov, J. K.; Siahrostami, S.; Wang, H. Highly Selective Oxygen Reduction to Hydrogen Peroxide on Transition Metal Single Atom Coordination. *Nat. Commun.* **2019**, *10*, 3997.
26. Tang, C.; Jiao, Y.; Shi, B.; Liu, J. N.; Xie, Z.; Chen, X.; Zhang, Q.; Qiao, S. Z. Coordination Tunes Selectivity: Two-Electron Oxygen Reduction on High-Loading Molybdenum Single-Atom Catalysts. *Angew. Chem. Int. Ed.* **2020**, *59*, 9171–9176.
27. Chang, Q.; Zhang, P.; Mostaghimi, A. H. B.; Zhao, X.; Denny, S. R.; Lee, J. H.; Gao, H.; Zhang, Y.; Xin, H. L.; Siahrostami, S.; Chen, J. G.; Chen, Z. Promoting H_2O_2 Production via 2-Electron Oxygen Reduction by Coordinating Partially Oxidized Pd with Defect Carbon. *Nat. Commun.* **2020**, *11*, 2178.
28. Wang, Y.; Shi, R.; Shang, L.; Waterhouse, G. I. N.; Zhao, J.; Zhang, Q.; Gu, L.; Zhang, T. High-Efficiency Oxygen Reduction to Hydrogen Peroxide Catalyzed by Nickel Single-Atom Catalysts with Tetradentate N_2 O_2 Coordination in a Three-Phase Flow Cell. *Angew. Chem. Int. Ed.* **2020**, *59*, 13057–13062.
29. Jasinski, P. A New Fuel Cell Cathode Catalyst. *Nature* **1964**, *201*, 1212–1213.
30. Hijazi, I.; Bourgeteau, T.; Cornut, R.; Morozan, A.; Filoramo, A.; Leroy, J.; Derycke, V.; Jousselme, B.; Campidelli, S. Carbon Nanotube-Templated Synthesis of Covalent Porphyrin Network for Oxygen Oeduction Reaction. *J. Am. Chem. Soc.* **2014**, *136*, 6348–6354.
31. Zhang, Z.; Sun, J.; Wang, F.; Dai, L. Efficient Oxygen Reduction Reaction (ORR) Catalysts Based on Single Iron

DOI: 10.31635/ccschem.021.202000590
CCS Chem. **2021**, *3*, 585–593

Atoms Dispersed on a Hierarchically Structured Porous Carbon Framework. *Angew. Chem. Int. Ed.* **2018**, *57*, 9038–9043.
32. Li, W.; Yu, A.; Higgins, D.; Llanos, B.; Chen, Z. Biologically Inspired Highly Durable Iron Phthalocyanine Catalysts for Oxygen Reduction Reaction in Polymer Electrolyte Membrane Fuel Cells. *J. Am. Chem. Soc.* **2010**, *132*, 17056–17058.
33. Wang, X.; Wang, B.; Zhong, J.; Zhao, F.; Han, N.; Huang, W.; Zeng, M.; Fan, J.; Li, Y. Iron Polyphthalocyanine Sheathed Multiwalled Carbon Nanotubes: A High-Performance Electrocatalyst for Oxygen Reduction Reaction. *Nano Res.* **2016**, *9*, 1497–1506.
34. Cao, R.; Thapa, R.; Kim, H.; Xu, X.; Gyu Kim, M.; Li, Q.; Park, N.; Liu, M.; Cho, J. Promotion of Oxygen Reduction by a Bio-Inspired Tethered Iron Phthalocyanine Carbon Nanotube-Based Catalyst. *Nat. Commun.* **2013**, *4*, 2076.
35. Zhang, X.; Wu, Z.; Zhang, X.; Li, L.; Li, Y.; Xu, H.; Li, X.; Yu, X.; Zhang, Z.; Liang, Y.; Wang, H. Highly Selective and Active CO_2 Reduction Electrocatalysts Based on Cobalt Phthalocyanine/Carbon Nanotube Hybrid Structures. *Nat. Commun.* **2017**, *8*, 14675.
36. Zhang, Z.; Xiao, J.; Chen, X.-J.; Yu, S.; Yu, L.; Si, R.; Wang, Y.; Wang, S.; Meng, X.; Wang, Y.; Tian, Z.-Q.; Deng, D. Reaction Mechanisms of Well-Defined Metal–N_4 Sites in Electrocatalytic CO_2 Reduction. *Angew. Chem. Int. Ed.* **2018**, *57*, 16339–16342.
37. Wu, Y.; Jiang, Z.; Lu, X.; Liang, Y.; Wang, H. Domino Electroreduction of CO_2 to Methanol on a Molecular Catalyst. *Nature* **2019**, *575*, 639–642.
38. Han, N.; Wang, Y.; Ma, L.; Wen, J.; Li, J.; Zheng, H.; Nie, K.; Wang, X.; Zhao, F.; Li, Y.; Fan, J.; Zhong, J.; Wu, T.; Miller, D. J.; Lu, J.; Lee, S.-T.; Li, Y. Supported Cobalt Polyphthalocyanine for High-Performance Electrocatalytic CO_2 Reduction. *Chem* **2017**, *3*, 652–664.
39. Jiang, Z.; Wang, Y.; Zhang, X.; Zheng, H. Z.; Wang, X. J.; Liang, Y. Y. Revealing the Hidden Performance of Metal Phthalocyanines for CO_2 Reduction Electrocatalysis by Hybridization with Carbon Nanotubes. *Nano Res.* **2019**, *12*, 2330–2334.
40. Zhang, X.; Wang, Y.; Gu, M.; Wang, M.; Zhang, Z.; Pan, W.; Jiang, Z.; Zheng, H.; Lucero, M.; Wang, H.; Sterbinsky, G. E.; Ma, Q.; Wang, Y.-G.; Feng, Z.; Li, J.; Dai, H.; Liang, Y. Molecular Engineering of Dispersed Nickel Phthalocyanines on Carbon Nanotubes for Selective CO_2 Reduction. *Nat. Energy* **2020**, *5*, 684–692.
41. Jiang, Y.; Lu, Y.; Lv, X.; Han, D.; Zhang, Q.; Niu, L.; Chen, W. Enhanced Catalytic Performance of Pt-Free Iron Phthalocyanine by Graphene Support for Efficient Oxygen Reduction Reaction. *ACS Catal.* **2013**, *3*, 1263–1271.
42. Frisch, M. J.; Trucks, G. W.; Schlegel, H. B.; Scuseria, G. E.; Robb, M. A.; Cheeseman, J. R.; Scalmani, G.; Barone, V.; Mennucci, B.; Petersson, G. A. *Gaussian 09*; Gaussian, Inc.: Wallingford, CT, **2009**.
43. Adamo, C.; Barone, V. Toward Reliable Density Functional Methods without Adjustable Parameters: The PBE0 Model. *J. Chem. Phys.* **1999**, *110*, 6158–6170.
44. Grimme, S.; Ehrlich, S.; Goerigk, L. Effect of the Damping Function in Dispersion Corrected Density Functional Theory. *J. Comput. Chem.* **2011**, *32*, 1456–1465.
45. Steinmetz, M.; Grimme, S. Benchmark Study of the Performance of Density Functional Theory for Bond Activations with (Ni,Pd)-Based Transition-Metal Catalysts. *ChemistryOpen* **2013**, *2*, 115–124.
46. Hariharan, P. C.; Pople, J. A. The Influence of Polarization Functions on Molecular Orbital Hydrogenation Energies. *Theor. Chim. Acta* **1973**, *28*, 213–222.
47. Gordon, M. S. The Isomers of Silacyclopropane. *Chem. Phys. Lett.* **1980**, *76*, 163–168.
48. Binning, R.; Curtiss, L. Compact Contracted Basis Sets for Thir-Row Atoms: Ga–Kr. *J. Comput. Chem.* **1990**, *11*, 1206–1216.
49. Andrae, D.; Häußermann, U.; Dolg, M.; Stoll, H.; Preuß, H. Energy-Adjusted Ab Initio Pseudopotentials for the Second and Third Row Transition Elements. *Theor. Chim. Acta* **1990**, *77*, 123–141.
50. Chan, K.; Nørskov, J. K. Electrochemical Barriers Made Simple. *J. Phys. Chem. Lett.* **2015**, *6*, 2663–2668.
51. Wang, Y.; Wang, M.; Zhang, Z.; Wang, Q.; Jiang, Z.; Lucero, M.; Zhang, X.; Li, X.; Gu, M.; Feng, Z.; Liang, Y. Phthalocyanine Precursors to Construct Atomically Dispersed Iron Electrocatalysts. *ACS Catal.* **2019**, *9*, 6252–6261.
52. Han, J. Y.; An, P. F.; Liu, S. H.; Zhang, X. F.; Wang, D. W.; Yuan, Y.; Guo, J.; Qiu, X. Y.; Hou, K.; Shi, L.; Zhang, Y.; Zhao, S. L.; Long, C.; Tang, Z. Y. Reordering d Orbital Energies of Single-Site Catalysts for CO_2 Electroreduction. *Angew. Chem. Int. Ed.* **2019**, *58*, 12711–12716.
53. Yan, C. C.; Li, H. B.; Ye, Y. F.; Wu, H. H.; Cai, F.; Si, R.; Xiao, J. P.; Miao, S.; Xie, S. H.; Yang, F.; Li, Y. S.; Wang, G. X.; Bao, X. H. Coordinatively Unsaturated Nickel-Nitrogen Sites towards Selective and High-Rate CO_2 Electroreduction. *Energy Environ. Sci.* **2018**, *11*, 1204–1210.
54. Dai, L.; Xue, Y.; Qu, L.; Choi, H. J.; Baek, J. B. Metal-Free Catalysts for Oxygen Reduction Reaction. *Chem. Rev.* **2015**, *115*, 4823–4892.
55. Jia, Y.; Zhang, L.; Zhuang, L.; Liu, H.; Yan, X.; Wang, X.; Liu, J.; Wang, J.; Zheng, Y.; Xiao, Z.; Taran, E.; Chen, J.; Yang, D.; Zhu, Z.; Wang, S.; Dai, L.; Yao, X. Identification of Active Sites for Acidic Oxygen Reduction on Carbon Catalysts with and without Nitrogen Doping. *Nat. Catal.* **2019**, *2*, 688–695.

DOI: 10.31635/ccschem.021.202000590
CCS Chem. **2021**, *3*, 585–593